

# Sliced-pupil grating: a novel concept for increasing spectral resolution

E. Sánchez-Blanco<sup>a</sup>, M. García-Vargas<sup>a</sup>, M. Maldonado<sup>a</sup>, J. Gallego<sup>b</sup>, A. Gil-de-Paz<sup>b</sup>, E. Carrasco<sup>c</sup>,  
A. Pérez<sup>a</sup>, I. Martínez-Delgado<sup>a</sup> & J. Zamorano<sup>b</sup>

<sup>a</sup>FRACTAL S.L.N.E., C/ Tulipán 2, p13,1A. Las Rozas de Madrid, Madrid (Spain);

<sup>b</sup>GUAIX group, Dept. Astrophysics, Univ. Complutense, Avda. Complutense.28040 Madrid (Spain);

<sup>c</sup>INAOE, Luis Enrique Erro # 1, Tonantzintla, Puebla (México)

## ABSTRACT

This paper presents the opto-mechanical design of a novel spectroscopic element – sliced pupil grating – that allows increasing the spectral resolution while keeping the instrument geometry. The concept is based on “cutting” the pupil into different slices by placing a number of prisms at the two sites of a VPH grating. The independent beams are guided through a precise opto-mechanical assembly to assure the recombination of the individual images on the detector within the available error budget, producing a single spectrum. To probe the feasibility of the concept, we have designed and manufactured a 3-slice prototype for an already-built spectrograph (Elmer, for the GTC 10-m telescope).

**Keywords:** spectrograph, spectral resolution, sliced-pupil, Astronomy, instrumentation, VPH

## 1. INTRODUCTION

Most optical telescopes are demanded to have an imaging camera and spectrograph running as work-horse instrument. For compactness, a fixed and straight geometry is widely used. Due to this reason, the angle of incidence on the grating is very limited and the attainable resolving power,  $R$ , is usually lower than 5000. We show a strategy that can allow multiplying by three or four the spectral resolution of current spectrographs. In addition, there were few spectrographs providing mid-resolution ( $R \sim 10000 - 20000$ ) in professional observatories and none of them can simultaneously provide a lower ( $< 5000$ ) or a higher regime ( $> 50000$ ) simultaneously. One of the reasons for that is the difficulty, in the optical design, of having different spectral resolutions regimens sharing the same geometry. This problem becomes even more relevant in large and giant telescopes, affecting from manufacturing problems in large pupil elements. The standard solutions, depending of the target spectral resolution, have been the use of echelle gratings, which implies to have a single or a much reduced number of observed objects, or the use of grism-type elements, by accommodating prisms at both sides of a transmission grating (VPH-type for throughput optimization) in order to increase the incidence angle on the grating and therefore the spectral resolution. However, the problem with this extended concept is that in these pupils, the prisms needed to reach high angles at high resolution are too thick and complex, and the system becomes inefficient.

We have developed the opto-mechanical design of a novel spectroscopic element – the sliced pupil grating – that allows increasing the spectral resolution while keeping the angle between collimator and camera, and therefore the same geometry. The concept is based on “cutting” the pupil into different slices by placing a number of prisms at the two sites of a VPH grating. The independent beams are guided through a very precise opto-mechanical assembly to assure the recombination on the individual images on the detector within the available error budget to produce a single spectrum.

To probe the feasibility of the concept, we have designed, manufactured and tested a prototype unit able to produce high resolution ( $R, \lambda/\Delta\lambda \approx 10000$ ) in the visible range (centered at  $H\alpha$  6563Å) in an already-built instrument (Elmer [2] for the GTC 10-m telescope) originally designed for  $R=2500$  (for a 0.6” wide slit) in Littrow configuration, and with straight in-line collimator-camera geometry ( $0^\circ$  incidence angle on pupil). This prototype has been built with three slices over an 89mm pupil aperture. We have performed the components’ individual tests as well as the system assembly at the Laboratory for Advanced Scientific Instrumentation, LICA, at the Universidad Complutense de Madrid (hereafter UCM). As a next step to use this concept in spectrographs for large and giant telescopes our group has designed a model of a 2-slice grating for the instrument MEGARA [1], a fiber-fed IFU and multi-object spectrograph for the GTC 10-m telescope. This will allow having resolutions of  $R=5600, 10000$  and  $17000$  with the same geometry, being the latest configuration obtained thanks to the sliced-pupil grating. MEGARA is lead by UCM (Spain), and the sliced-pupil gratings shall be designed by FRACTAL and manufactured by Wasatch (VPHs) and INAOE (prisms and windows).

## 2. OPTICAL DESIGN

### 2.1 Optical design and concept

The concept is shown in Figure 1 (left). The unit is composed of six prisms (three on each side) and the grating, consisting on a VPH hologram sandwiched between two flat windows. The VPH has 3400 lines/mm ( $R=10000$  at first order).

In order to obtain the high AOI on the grating for the required resolution, three prisms will slice the beam in three portions. A TIR on the upper faces of these three prisms will supply the required incidence angle on the grating. A gap among the three prisms at either side will be used to avoid tunnel transmission among the prisms. The prisms seat on the gel-coupled VPH window. After diffraction the beam will be redirected again using TIR on 3 new prisms to the camera.

The camera (Figure 1, right) has four elements: two doublets and two individual lenses, with a focal length of 124mm. In the image different colors indicate different wavelengths. The material for the window and prisms is fused silica.

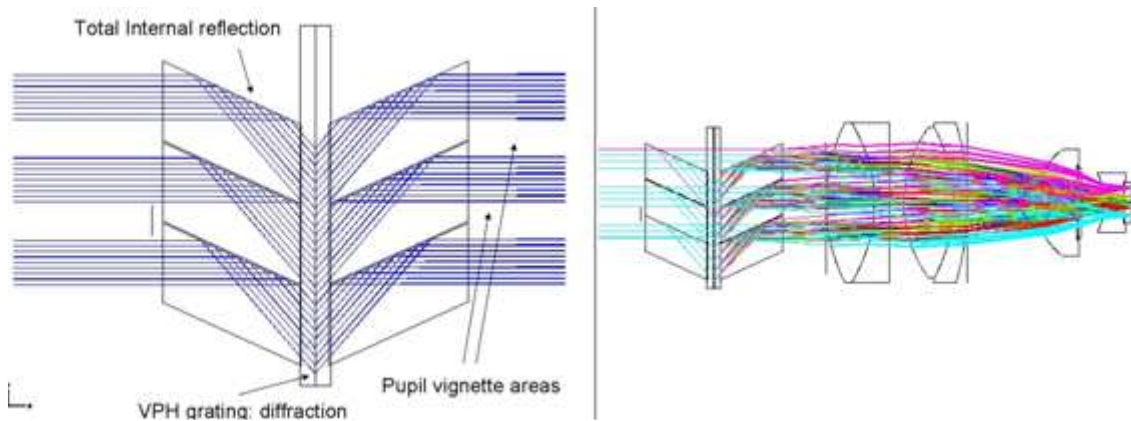


Figure 1. Left: Sliced Pupil Grating concept. Right: layout of the slicing device with Elmer camera.

The unit is placed at the pupil (89mm  $\varnothing$  size) with a clear aperture of 105mm that allows covering all unvignetted field at the edges. Nevertheless, as the pupil is sliced in three pieces to minimize assembly difficulties, some parts of the pupil's flux are lost (producing vignetting). In fact only 62% of the incoming pupil beam passes through the system. The unit is also de-centered 4mm to accommodate the beam, going downwards after the TIR reflection the unit. Other designs, which have been optimized together with the main instrument, have allowed us to get vignetting as low as 18%.

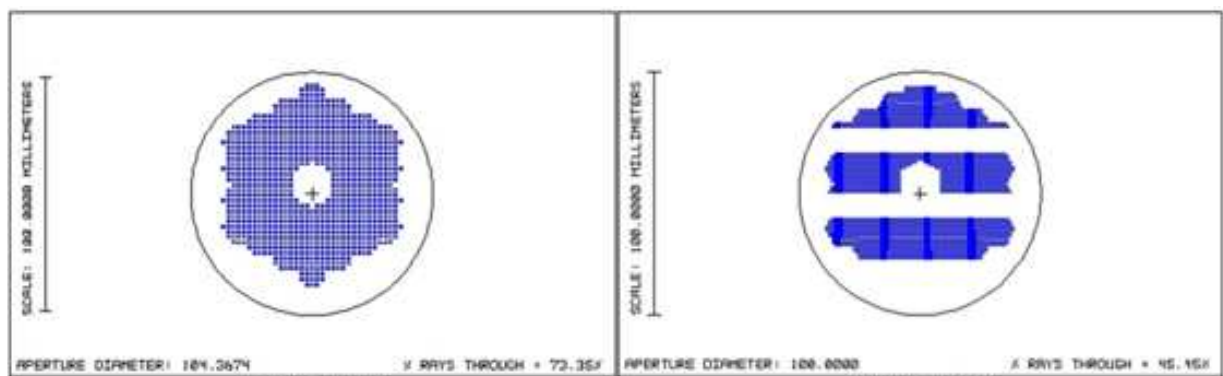


Figure 2. On the left the nominal pupil of the central field at 656.3nm before crossing the dispersive element. On the right the vignetted areas are shown. Only 62% of the pupil area is expected to pass through the aperture.

Difficulties arise when we consider that after the beam slicing, we have to recombine the three different paths. In fact the perfect scenario would be to recover the path without delays among the beams. We do not intend to recover this coherence as the beam through the atmosphere is already corrugated. We can estimate the wavefront rms (equation 1) as:

$$\text{FWHM (rad)} = 0.98 \times \left( \frac{\lambda}{R_0(\lambda)} \right) \quad (1)$$

, where  $R_0$  (Fried parameter) is 22cm,  $\lambda = 656.3$  nm and  $\text{FWHM} = 0.6''$ . The wavefront rms is given in equation 2.

$$\sigma^2 = 1.023 \left( \frac{d}{R_0} \right)^{\frac{5}{3}} \quad (2)$$

, for this seeing and a 10.4m telescope. The result for  $\sigma = 25$  radians, is about  $4\lambda$  rms, or  $12\lambda$  P-V. Our strategy is based on common image stacking not far from the atmospheric maximum departure. As the unit will work above the diffraction limit, we do not expect large effects due to the beams interference (only few percent).

## 2.2 VPH design and performance

The hologram parameters and windows were computed to give  $R=10000$  at 656.3nm. The hologram thickness was minimized to avoid a high dependence in the efficiency for the out of Littrow angle (Figure 3). The VPH has 3400 lines/mm. The windows were done in fused silica to match as much as possible the dichromated gelatin index ( $n=1.27$ ) to minimize insertion losses between the window and the gelatin. The angle of incidence within the gelatin is given by the standard grating equation at Littrow configuration (equation 3)

$$2dn \sin \beta_m = m\lambda \quad (3)$$

Where  $m$  is the spectral order,  $\lambda$  is the wavelength (656.3nm),  $d$  is the spacing between each groove ( $1/d = 3400$  lin/mm), and  $n=1.27$  is the gelatin refractive index. With this values  $\beta_m = 61.45^\circ$  within the hologram.

When the light goes from the gelatin to the fused silica substrate, we apply the Snell law (equation 4).

$$n_{\text{gelatin}} \sin(\beta) = n_{\text{silica}} \sin(\alpha) \quad (4)$$

Where  $n$  (silica at 656 nm) = 1.4563, so the incidence beam is  $\alpha = 50^\circ$ . This is the incidence angle provided by the TIR reflection in the prism. Finally, as the instrument cannot transmit below 350 nm, no second order is seen at 656.3 nm.

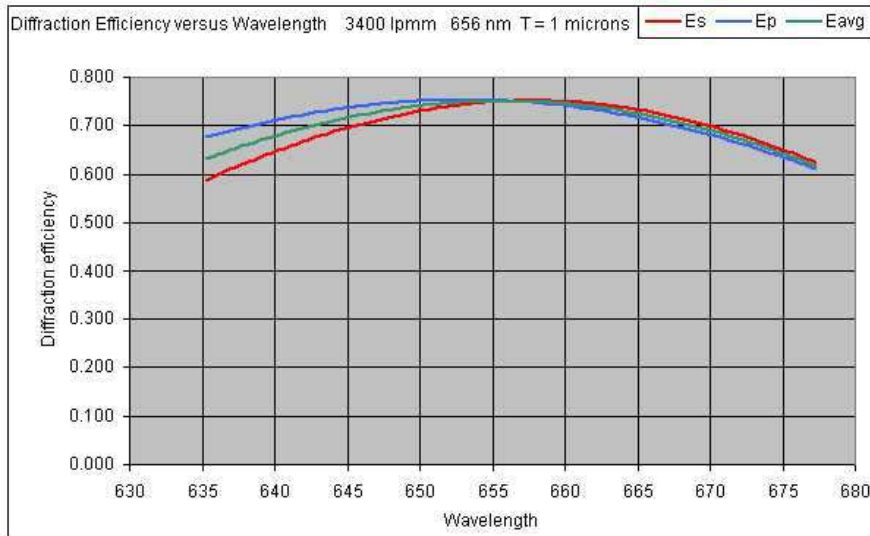


Figure 3. Efficiency performance of the proposed VPH grating (Provided by Wasatch Photonics)

## 2.3 Spectral resolution performance

The Zemax model was evaluated in a combined sequential mode for the instrument with a non-sequential mode for the dispersive element (required as the beam is sliced at the pupil in simultaneous paths). The nominal resolution (for the camera shown in Figure 1) is computed by measuring the centroids (position) of the image between 655.8nm and

656.8nm at the central field. The centroid difference is 703.8 $\mu$ m. Having a CCD with 15 $\mu$ m pixels and 3-pixel resolution element we compute the expected resolution  $R = \lambda / \delta\lambda = 10.264,5$  at 656.3nm.

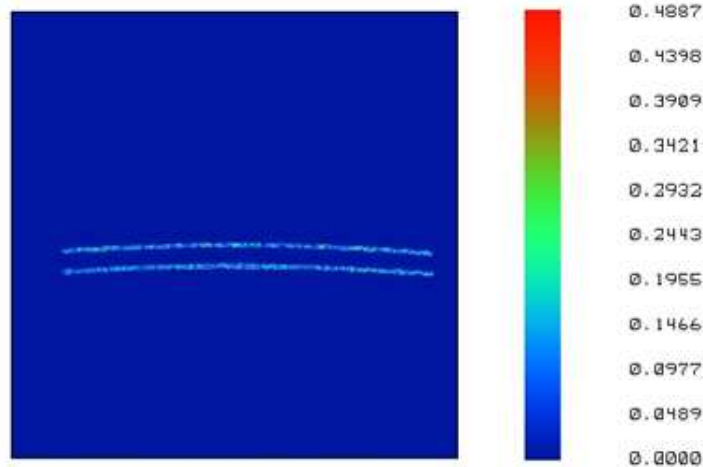


Figure 4. Bitmap image analysis of a 3 arcmin long slit illuminated at 655.8nm and 656.8nm.

## 2.4 Image quality and Efficiency performance

Zemax physical optics module cannot be used in a complex non sequential model so that diffraction effects due to the beam recombination of the pupil cannot be analyzed. Image stacking has to guarantee 0.6" images of the entrance slit on the detector. The Image quality requirement is to have the encircled energy diameter, measured at the 80% level ( $EED_{80}$ ) in less than three pixels (45 $\mu$ m),  $EER_{80} < 22.5\mu$ m. All fields and wavelengths are within requirements except at the 4' long-slit edges. This implies that this grating can be used not only in the standard 3' length slit but also with a special slit over the whole FOV of the camera (4.2') or in the slit-less mode. The nominal image quality considers a perfect system only with design errors. The image stacking will introduce some degradation that will bring the performance between the requirement and the theoretical value. A very good stacking could allow using a 0.4" slit boosting the resolution to  $R=15.000$  and having the image quality within two pixels.

We expect an efficiency of 50% for this (all effects included), which is competitive compared to existing echelle designs (with overlapped orders). The beam will cross the following interfaces: (a) Two air /glass interfaces, a standard V coatings has been considered, with a double layer AR coating, assuming 0.5% reflectance per interface; (b) A TIR in the upper prism face has an efficiency of 100% in reflectance; (c) Four glass-gel /gel-glass interfaces. This is required to avoid a second TIR in the interface between prism and window. The optical coupling is a gel matched to fused silica.

Figure 3 shows the VPH overall efficiency. This includes diffraction efficiencies and absorption losses in the interface. The largest loss comes from the unused parts of the pupil once it has been sliced. A 38% flux is lost due to this effect. To decrease this vignetting we should increase slicing, implying more manufacturing and assembly complexity for stacking.

## 2.5 Ghost and stray light analysis

The ghost generation is due to bounces between surfaces out of the nominal path. The light coming from each bounce depends on the interface reflectivity. Therefore, the less number of bounces the higher the ghost flux. To have a reflection back, the number of bounces has to be a multiple of two bounces. The front and back surfaces of the prisms are flat and normal to the nominal beam. This was done intentionally to facilitate prism manufacturing, stacking alignment and the final surface testing. The flat surfaces means that produced focused ghost spectra were carefully analyzed. We have done an exhaustive ghost analysis that is available under request.

Regarding stray light and baffling, as the nominal system is having an efficiency of 54%, we have to guarantee that the lost flux will not reach the detector and will be absorbed before creating a scattered halo. We have analyzed with a pure non-sequential model the different geometries and order to be able to identify the undesired paths, which are mostly due to reflections in the bottom prisms, sometimes coming from a part of the unused pupil. The strategy for stray light

control will consist on blocking the unused areas of the pupil before entering the disperser. Moreover, the unused parts of the prisms, bottoms and sides will be black painted (except for the support areas).

## 2.6 Error Budget. RMS Wavefront error

The single-slice error budget contains the rms wavefront error information within each of the 3 single paths. All errors are considered except piston and tilt, which are analyzed in the stacking error budget. A summary is shown in Table 1.

Table 1. Wavefront error budget summary for each path. Nominal performance includes GTC + Elmer + sliced pupil grating

ITEM	$\sigma$ (waves at 656.3 nm)	Verification
Nominal performance:	0.77	Zemax: Nominal design
Prism glass homogeneity	0.26	Analytical model
Prism error: Surface quality	0.32	Analytical model
VPH fabrication	0.31	Analytical model
Margin	0.62	
TOTAL	1.06	

This analysis allows specifying glass type, surface quality and VPH WFE. The expected degradation is of 38% over the nominal value. EED<sub>80</sub> requirement is set to be lower than 26 $\mu$ m for all fields and wavelengths and the requirement allows degrading up to 45 $\mu$ m (3 pixels) implying 73% degradation. As the camera and detector configuration are achieving EED<sub>80</sub> within 2 pixels, this error budget meets the requirements.

Nominal performance: The error generated at the pupil is common to all fields. We assume as baseline error the wavefront rms of a centered field at 656.3 nm. We set up a merit function on wavefront rms, by using the rectangular array pupil integration method and removing the vignetted rays of the telescope serrated pupil, giving  $\sigma=0.77$ waves.

Glass errors: Index error is not a major contributor as the incidence angle is obtained from reflection. Standard refractive index tolerances are valid for this purpose. Homogeneity has to be specified in order to avoid large phase delays. The total length within the prism glass is 120 mm. The contribution is computed as: OPD = Optical Thickness x IndexHomog. For a homogeneity error  $\pm 5 \times 10^{-6}$  ppm, P-V =  $\pm 0.6\mu$ m (0.91 $\lambda$  at 656.3 nm). The average rms is estimated as PV/3.5, thus  $\sigma=0.26$ . As the prism works in all directions, the homogeneity was required in the 3 dimensions.

Prism surfaces: Six surfaces are used in two prisms along the path. The surfaces for each prism are: one air-glass surface, one top surface that is used in TIR, and one back surface optically coupled with a silica gel. Every surface has a different specification regarding applied area and surface. The top surfaces have the highest sensitivity to errors due to reflection inside the glass. The rms is estimated as P-V/3.5. Then the total contribution is squared averaged. The surface quality specification was given with these results and considering a margin of 4mm around the edges.

VPH fabrication: We had to avoid large pupil de-centering due to envelope constrains. Thus, the glasses used for sandwiching the grating are thin (5 mm). Due to the large pupil size (89mm) and thin glasses, we expect deformation in the wavefront. The WFE will share common low order features for all paths. We admit focus error (compensated with the instrument focus mechanism), and a partial compensation of spherical aberration (up to 50%). High order irregularity cannot be compensated and a more strict specification was placed. The ordered VPH has a WFE over the irregularity value but as these surfaces will be sandwiched with the prisms we expect to partially compensate this effect. The number of lines is given with  $\pm 3$  lines/mm error and a wedge error on the VPH after assembly of 2 arcmin. Both effects introduce a small shift of the spectrum in the detector without image degradation.

## 2.7 Stacking Error Budget

This budget refers to the combination of the three paths. The components are the centroid displacement considered in the x (spatial) and y (spectral) axis. The budgeted error is 15  $\mu\text{m}$  if we do not want to degrade the slit profile more than 10%. A summary of the main contributions is shown in Table 2.

Table 2. Stacking Error Budget. Nominal performance includes telescope, instrument and grating

ITEM	Image centroid x-axis ( $\mu\text{m}$ )	Image centroid y-axis ( $\mu\text{m}$ )	Verification
Nominal performance	0	0	Design
Prism manufacture: angles and //	-	0	Analysis / Zemax
Prism assembly.	< 21	< 5 gel stacking residuals	
VPH fabrication	0	0	
TOTAL	< 21	< 5	residuals

Nominal performance: In a perfect unit there are no stacking errors and the three images are coincident.

Prism manufacture: The manufacturing differences in the angles among the three prisms at either side of the VPH introduce an error in the image stacking. Figure 5 shows the angles that produce this error.

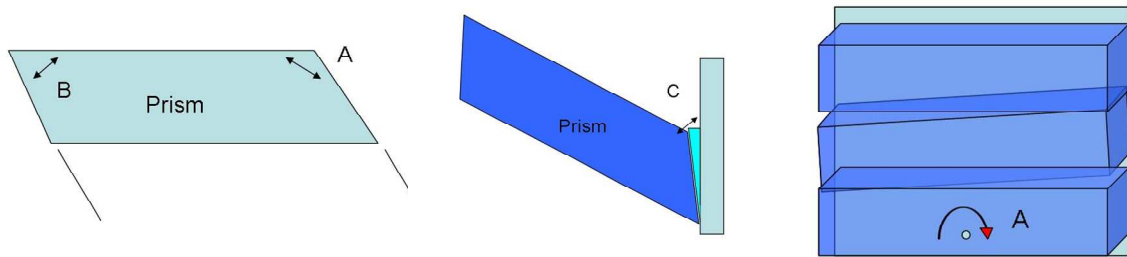


Figure 5. Left: layout showing the tolerated angles for image movement in the spectral axis. Center: wedge error if the prisms were badly optically coupled to the VPH. Right: mounting error (tilt in A) when a prism is mounted stacked on top of the next one.

For stacking error budget in the spectral axis, we will consider the worst case, B and A angles add in the worst direction for both prisms. A sensitivity analysis is shown in Table 3. Notice that A angle is almost 6 times more sensitive than B. The resulting tolerances are extremely tight, with a very high impact in cost. The strategy to compensate for this source will consist on the manufacture of a single slice and once is finished cutting the three prisms from it. With this concept we can guarantee no error among the three prisms regarding angles. The prisms were manufactured from single bars whose faces were polished. Afterwards three prisms were cut from each bar (also each bar was obtained from a single piece). The acceptance measurements indicate angle identity errors under the measurement capabilities ( $\pm 2$  arcsec).

Table 3. Sensitivity for prism errors and manufacturing tolerance for the prisms at each side to guarantee image stacking

	Sensitivity Analysis		Manufacturing	
	Tolerance	Image shift ( $\mu\text{m}$ )	Tolerance	Image shift ( $\mu\text{m}$ )
Prism 1. A angle	1'	107	3.5"	6.38
Prism 1. B angle	1'	18.5	3.5"	1.12
Prism 2. A angle	1'	107	3.5"	6.38
Prism 2 B angle	1'	18.5	3.5"	1.12
Total				15

## 2.8 Assembly tolerances and compensation strategies

Two mounting tolerances are important when assembly: C affects the spectral direction while A affects the spatial direction. The sensitivity analysis is shown in Table 4. It can be seen that the tolerances in angle A are twice more sensitive as the tolerances in angle C. Table 4 also shows the tolerances to fulfill the error budget in the prism assembly.

Table 4. Sensitivity analysis for mounting and assembly tolerances for the prisms to guarantee image stacking

	Mounting sensitivity analysis		Prisms Assembly Tolerances		
	Tolerance (')	Image shift ( $\mu\text{m}$ )	Tolerance (arcsec)	Image shift ( $\mu\text{m}$ ) spectral direction	Image shift ( $\mu\text{m}$ ) spatial direction
Prism 1. A angle	1'	38	11.9"		7.5
Prism 1. C angle	1'	18.5 (spectral)	7.9"	2.5	
Prism 2. A angle	1'	38	11.9"		7.5
Prism 2 C angle	1'	18.5 (spectral)	7.9"	2.5	
Total					15

These tolerances have to be translated to dimensional values. In the case of the C angle (for the optical coupling), the face is 24 mm long, thus 7.9" gives a maximum  $0.9\mu\text{m}$  wedge. This is a very tough target. The coupling is required as the high incidence angle is well within the TIR condition even using standard coatings, so we have decided to use a gel to optically coupled surfaces. The prisms have to accommodate for many hours under getting stabilized with the two surfaces in contact. The coupling gel is the Cargille 0607 soft gel. In the case of the A angle, the length of the prism is 120 mm, so 11.9" represents  $7\mu\text{m}$  in wedge. As the mother prism (cut in three pieces) is 330 mm we have a specification value of  $20\mu\text{m}$ , which meets the requirement. Shims are used to compensate for the A angle between the adjacent prisms. Standard thickness of  $10\mu\text{m}$  is available and we would only have a small excess of stacking error in the spatial direction, which has no effect in the spectral resolution.

## 2.9 Compensators and risk management summary

Once the error budget has been set up, different compensation strategies can be used for the manufacture and assembly procedures, which specifically apply to the stacking error budget.

Prism manufacture: Each group of three prisms is extremely sensitive (few arcsec) to the differences among angles. The manufacture of two large single bars and cut three pieces from them was used.

Prism assembly: Regarding the C angle, all prisms are coupled with a non curing gel while being pressed against the grating surface. This surface is a reference plane (thus no over constrain in the lateral supports). Nevertheless as the spatial axis is referenced when piling up the prisms, shims have to be placed with the aid of an alignment telescope in order to guarantee the stacking of the images. The  $10\mu\text{m}$  shims will allow and alignments better than 17 arcsec or  $21\mu\text{m}$  on the detector in the worst case scenario.

Image quality: Although with the explained procedure, there is no need of any compensation except for the instrument focus, in case we could not obtain the required performance regarding image quality or stacking, the device foresees the adaptation of a phase plate specifically matched to compensate for any wavefront error to virtually a perfect system. As we are working at the pupil and in a short wavelength range, almost any transmission plates would correct errors (e.g. Lithographic fused silica -Jenoptik- or index matching polymeric plates -Lexitec) at a penalty of a manufacturing over-cost (6000€- 9000€ is the plate's cost) and about 2% transmission loss.

Finally, to give an idea of the manufacturing cost and time of the whole unit, a 3 sliced-pupil grating for a 90mm pupil can cost about 70.000 € and 1 year from ordering to the final assembly and tests. Manpower effort for design and testing has to be added to this estimation.

### 3. OPTO-MECHANICS DESIGN AND ASSEMBLY

In order to place the optical elements in their exact position within the instrument optical path, they must be inserted on a mount that interfaces with the Elmer instrument prisms wheel.

This mount allows placing the different optical elements in its exact position relative to each other as well as locating the whole grating with precision onto the optical path, both defined by the optical design. The mount has been designed to absorb the differential thermal dilatations of the optics with respect to the aluminum mount, maintaining its performance, and preventing surface stresses that may affect the transmission.

#### 3.1 Mechanical interfaces review

The optical design presented in the previous section is quite symmetrical, with a central flat window and three prisms on either side. The hologram is embedded in the central element, which in fact is a sandwiched window. The mount must leave an optical aperture of  $\varnothing 105$  mm, with its centre on the optical axis of the instrument. It must also comply with the envelope provided on the prism wheel, and keep its maximum size between limits defined by the distance between the camera and the filters wheel. It is desirable that the mount stays as near as possible to the camera to assure the best aperture without vignetting and prevent stray light. Figure 6 is a drawing showing the location in the instrument.

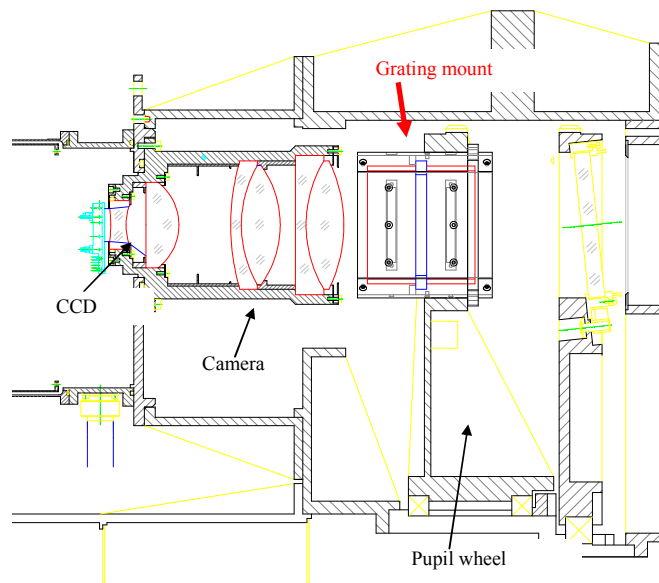


Figure 6. Drawing of the location of the grating on the instrument

The correct interface is guaranteed by the fact that there are already some dispersive elements mounted on the instrument, and in this mount we provide the same dimensions. This mount will have a shorter length than other elements (such as standard VPH units with 2 large prisms, one at each side) and the method of mounting and dismounting it from the wheel is by using the same tool. Its weight will also be smaller.

#### 3.2 Description of the mount

Figure 7 shows a 3D model of the mount. It has a total of 26 parts, 23 screws and 24 compression springs. All parts are manufactured on aluminum alloy (Al-Mg-Si) 7075-T6 or similar. They are given a matte black-anodized surface

treatment to provide a protective layer against corrosion and prevent stray light within the mount. They all can be manufactured with standard mechanical workshop machines. All screws and springs are made of stainless steel. The screws are socket head DIN7991, of different lengths.

The main body is made of 7075-T6 aluminum alloy. It is the biggest part of the mount and provides the interface with the instrument wheel with a tolerated hole and groove that fit on correspondent alignment pins. On its inner surface there will be mechanized two axial reference surfaces that provide a precise location with respect to the instrument I/F. There will also be a vertical reference that provides restriction on rotation around the optical axis. This is critical due to the alignment of the lines of the grating. The flat sandwiched window with the hologram is located into the mount. It is secured on its position with two axial support pieces, screwed to the mount, so it can be handled to locate the following optical and mechanical elements on the VPH grating. This support piece also gives certain lateral fixation to the hologram window and works as a flexure to prevent stress on the hologram.

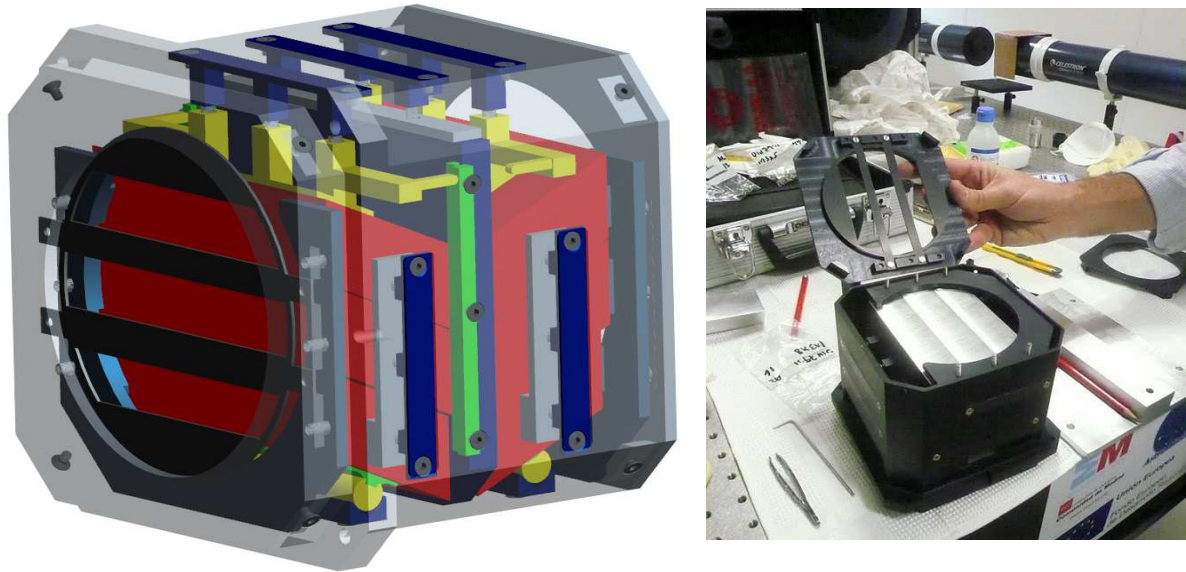


Figure 7. Left, 3D view of the overall grating design. Right, real element with aluminum dummy prisms during tests

The prisms are located on the mount. Its mounting reference surface is the hologram window itself. The vertical support is a pivot device that does not disturb the perfect coupling between the prisms surfaces and the hologram surface. Also for this reason, there will be a very small and thin shim between each two prisms. The pivot device is comprised of three parts: a part that interfaces with the prism, joined with screws to a cylinder that rolls on a V-groove. The cylinder and the V-groove have better than standard surface quality (N6 instead of N7) to reduce friction.

The prisms are pressed against the pivot support with another part, located on the opposite side of the mount, which holds three springs. The load of the springs has been calculated as being two times the weight of the prisms (our BK7 prisms, with a density of 2,52 g/cm<sup>3</sup>, have a total weight of the 3 prisms of 1184 grams, or 11,62 N, so that each of the 3 screws must apply a load of around 8 N). The elongation of the spring is determined by the depth of the holes of both parts #3 and # 4. The latter is screwed to the outer side of the Main Body while passing through a hole provided for it. The location of the springs coincides with the lines of centers of gravity of the prisms.

All the surfaces that make contact with the prisms shall be covered with tape to prevent direct metal-glass contact. The vertical fixation of the hologram follows the same design. An intermediate aluminum plate is pushed against the hologram side by 2 springs. To guarantee the positioning and facilitate the integration of this support plate, the axial reference surface was enlarged to “capture” this plate.

On the lateral direction, the mount also has an elastic support. There is one fixed part on one side and on the opposite side, another part that presses with three springs against the first one. Due to the decentering of the system, the lower prism is smaller than the other two. This has been considered in the design of the parts of the lateral support. These supports have the same springs used in the vertical support.

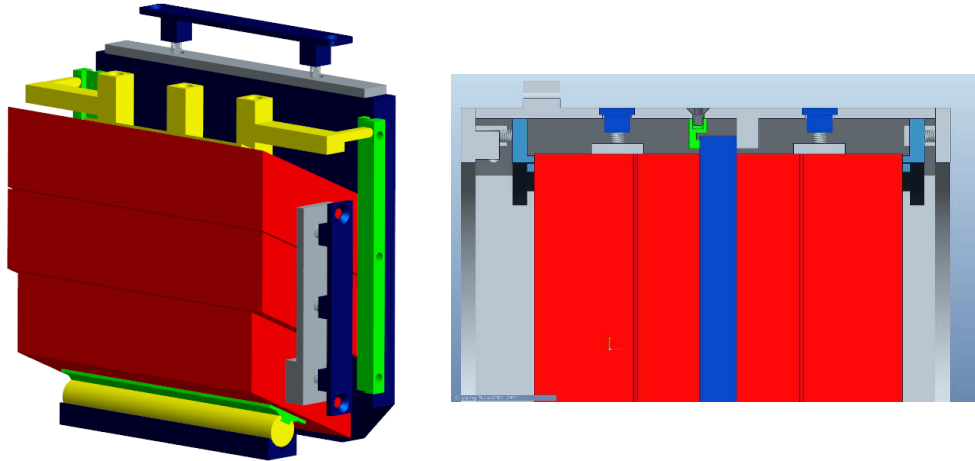


Figure 8. Left, several supports of the prisms, notice the pivot device at the bottom. Right, cut showing assembly details.

On the axial direction, the whole system (hologram + prisms) is fixed by another spring-loaded part. It had left an inner free diameter of  $\text{\O}105$  mm. To obtain a more stable position, instead of pretending to establish a full-surface contact, there will be mechanized 6 protrusions that push the prisms as near as possible to their centers of gravity.

There are six springs. The last elements to introduce in the mount are the baffles. We have two aperture baffles, one on each side of the mount, and a specific mask that prevents ghosting on the prisms faces. This is an aluminum alloy plate with a thickness of 1mm. Each baffle is joined to the mount with 4 screws, which are placed on the corners because there is no room enough to place them on the front. The outer baffles are quite similar, being the only difference a small rectangular protrusion made on the entrance baffle to allow using the same springs on both sides and holding the mask.

#### 4. CONCLUSIONS

We have designed a novel pupil element called sliced-pupil grating, able to increase the spectral resolution by cutting the pupil with different prisms, perfectly aligned, placed at both sides of a sandwiched-VPH, and then recombining the individual beams and stacking them on the detector to get a single image. We have manufactured and tested a real unit that shows the goodness of the concept whose results will be presented in a further paper. The use of this element allows to increase the resolution of already-built astronomical spectrographs without changing the geometrical configuration by a factor up to 4, and also, in new instruments, sliced pupil elements allow an efficient system for high resolution spectrographs as well the possibility of having very different spectral resolutions with the same optical configuration, what has advantages not only from the scientific point of view, but also for the optical design and calibration.

#### 5. REFERENCES

1. Carrasco, E., Sánchez-Blanco, E., García Vargas, M.L. Gil de Paz, A., Gallego, J., Páez, G., Zamorano, J. & Castro J. "Optical design for MEGARA: a multi-object spectrograph for the GTC", these proceedings.
2. Cabrera-Lavers, A.; García-Vargas, M.; Martín-Fleitas, J.; Kohley, R.; Sánchez-Blanco, E.; Hammersley, P.; Maldonado, M. "Elmer spectroscopy: Characterization and performance results from the pre-shipping acceptance tests", RMxAC, Vol. 29, pp. 137-137 (2007)

*Acknowledgments: The sliced-pupil grating prototype was funded by FRACTAL, CAM [project 22/2009 for Aero-spatial Innovation] and UCM through the MICINN project AyA-10368. The presentation in ICO-2011 has been co-funded by Spanish MICINN under the Consolider-Ingenio 2010 Program grant CSD2006-00070: First Science with the GTC (<http://www.iac.es/consolider-ingenio-gtc>) and by CDTI VIENTOS project (IdC-20101106), who is also funding further studies for application of sliced-pupil grating in the Instrumentation of the next generation of giant telescopes.*